Numerical studies on the effect of normal-metal coatings on the magnetization characteristics of type-II superconductors

G. J. Carty
Department of Physics, Superconductivity Group, University of Durham, South Road, Durham DH1 3LE, United Kingdom

M. Machida
Center for Promotion of Computational Science and Engineering, Japan Atomic Energy Research Institute, Higashi-Ueno, Taito-ku, Tokyo 110-0015, Japan

D. P. Hampshire
Department of Physics, Superconductivity Group, University of Durham, South Road, Durham DH1 3LE, United Kingdom
(Received 30 July 2004; revised manuscript received 18 January 2005; published 19 April 2005)

Magnetic properties of superconductors coated with metals of arbitrary resistivity ρ_N are calculated using the time-dependent Ginzburg-Landau equations in which both T_c and ρ_N vary. As ρ_N in the coating is reduced, the initial vortex penetration field $H_p(\rho_N)$ does not decrease monotonically from the insulating (Matricon) limit to the extreme metallic (Bean-Livingston) limit, but has a minimum value $H_{p(\min)}$ below the extreme metallic value. The minimum occurs because the barrier is weakened by proximity-effect penetration of superelectrons into the coating which only occurs at finite resistivity. In an applied magnetic field, local depressions in ψ nucleate in the coating which do not have the well-known quantum of magnetic flux ($h/2e$) until they have crossed the coating and entered the interior of the superconductor. When $T=0$ and T_c of the normal metal coating is zero, the minimum vortex penetration field $H_{p(\min)} \approx 0.76\kappa^{-1.17}H_{c2}$ which occurs for a coating resistivity $\rho_N \approx 1.1\kappa^{-0.6}\rho_S$. For $T>0$ the minimum is attenuated. Adding a thick weakly superconducting S' layer between the superconductor and normal metal coating reduces the irreversibility markedly.

DOI: 10.1103/PhysRevB.71.144507 PACS number(s): 74.20.De, 74.25.Ha, 74.25.Op

I. INTRODUCTION

Within the past decade, the CPU clock speed of PCs has increased by about 100 times, and the use of parallel processing has increased supercomputer speed by up to 3 orders of magnitude, making many problems accessible to solution by computational techniques. In addition, a Crank-Nicolson[1] algorithm established for solving the superfluid Gross-Pitaevskii equations[2] has been adapted for solving the time-dependent Ginzburg-Landau equations,[3] which provides a further improvement in efficiency of one or two orders of magnitude. These improvements permit the use of TDGL computation to model superconductors with high finite κ values in contact with nonsuperconducting materials.

The phenomenological TDGL equations provide a way of modeling superconductivity more complete than simple macroscopic models,[4,5] but without the extreme complexity of microscopic theory which makes such calculations impractical for the mixed state. The TDGL equations have been used to calculate *I-V* characteristics for superconductors with insulating-boundary surface pinning[6] and with bulk pinning by point pinning sites.[7] The initial vortex penetration field of a superconductor with a notch[8] has also been investigated using TDGL theory, along with the current flow in a 3D layered superconductor.[9,10] Some of the systems considered in the literature consider spatially varying material properties by invoking a variation in the critical temperature T_c.[9–12]

The effect of surface barriers on superconductors is a phenomenon which has been researched in detail for most of the history of superconductivity. The effect of coatings on the surface critical field H_{c3} has been determined by using linearized equations to obtain H_{c3} as a function of coating resistivity.[13] The question of initial vortex penetration into a coated superconductor was first posed by Bean and Livingston,[14] and solved in the high-κ limit using London theory, and using 1-D Ginzburg-Landau theory.[15] The Bean-Livingston model is based on the competition between the attraction from an "image force" and repulsion due to the screening currents, and predicts an initial vortex penetration field $H_p \approx H_c$. Much later, it was confirmed computationally[16] that their result is valid for the extreme metallic limit irrespective of κ. The case of the superconductor with an insulating surface was solved by Matricon and Saint-James using the 1-D Ginzburg-Landau equations,[17] showing that H_p was noticeably higher than the Bean-Livingston value, due to the need to force the material normal at the insulating edge before fluxons can enter. This has more recently been followed by computational work[16,18] which confirmed the Matricon result.

This paper extends our understanding of coated superconductors from the insulating and extreme metallic limits to the case of superconductors coated with metals of arbitrary resistivity. These systems involve spatial variation of both T_c and normal-state resistivity ρ. The generalization of the computation to include spatially-dependent ρ necessitates implementation of internal boundary conditions, but enables the direct computational simulation of new classes of systems. Hence coated superconductors, polycrystalline bulk materials (where the grain boundaries may be nonsuperconducting) and superconducting composite conductors (which may in-

clude normal metal matrix materials) can all begin to be addressed computationally. Our aim in this work is to determine the effect of the surface barrier on the hysteretic magnetic response to an applied magnetic field. As part of our long-standing interest in bulk superconducting properties, we have also considered how best to eliminate the surface barrier from a superconductor. For this reason the properties of bilayer coatings, which consist of a weakly superconducting S' layer interposed between the superconductor and normal coating are calculated. This bilayer structure was chosen in light of the experimental findings[19,20] that the creation of a diffusion layer between a superconductor and its normal metal coating reduces the superconductor's magnetic irreversibility.

In Sec. II an overview of the time-dependent Ginzburg-Landau model is given, and the appropriate parameters based on normal-state material properties are determined. In Sec. III we discuss the general impact of symmetry considerations on TDGL computation, the numerical method itself, and how the calculations were optimized.

In Sec. IV we consider a superconductor coated with a normal metal. The magnetization characteristics themselves are calculated along with the initial vortex penetration field H_p and the hysteresis. The minimum possible H_p and corresponding ρ_N/ρ_S are also found. (ρ_N/ρ_S is the ratio of the coating resistivity to the normal-state resistivity of the superconductor.)

In Sec. V we consider the effect of introducing a weakly superconducting region between the superconductor and the normal metal coating. As for the single normal metal coating, complete magnetization loops and H_p values are calculated. The implications of all the results obtained are discussed further in Sec. VI. Finally, in Sec. VII we give a summary of the results and conclusions.

II. BACKGROUND THEORY

A. The TDGL equations

The work described in this paper involves Ginzburg-Landau computations on systems containing both superconductors and normal metals. As given in the literature the standard form of the TDGL equations is[21,22]

$$\frac{1}{\xi^2}(|\psi|^2-1)\psi+\left(\frac{\nabla}{i}-\frac{2e}{\hbar}\mathbf{A}\right)^2\psi+\frac{1}{D}\left(\frac{\partial}{\partial t}+i\frac{2e}{\hbar}\varphi\right)\psi=0, \tag{1}$$

$$\mathbf{J}_e=\frac{\hbar}{2e\mu_0\lambda^2}\mathrm{Re}\left(\psi^*\left(\frac{\nabla}{i}-\frac{2e}{\hbar}\mathbf{A}\right)\psi\right)-\frac{1}{\rho}\left(\nabla\varphi+\frac{\partial\mathbf{A}}{\partial t}\right). \tag{2}$$

The values of ξ and λ, which are the characteristic lengths for the order parameter and supercurrent, respectively, can be deduced from microscopic theory in the dirty limit:[23]

$$\xi=\sqrt{\frac{\pi\hbar D}{8k_B(T_c-T)}}, \tag{3}$$

$$\lambda=\sqrt{\frac{7\hbar\rho\zeta(3)}{4\pi^3\mu_0 k_B(T_c-T)}}, \tag{4}$$

where T_c is critical temperature, $D\left(=\frac{1}{3}v_F^2\tau\right)$ is diffusivity, ρ is the normal-state resistivity and ζ is the Riemann zeta function [$\zeta(3)\approx 1.202$]. Similarly there are two characteristic time constants $\tau^{\psi}_{(1)}$ and $\tau^{\mathbf{J}}_{(1)}$:

$$\tau^{\psi}_{(1)}=\frac{\xi^2_{(1)}}{D_{(1)}} \tag{5}$$

$$\tau^{\mathbf{J}}_{(1)}=\frac{\mu_0\lambda^2_{(1)}}{\rho_{(1)}} \tag{6}$$

ζ' is the ratio of the two time constants, given by

$$\zeta'=\frac{\tau^{\psi}}{\tau^{\mathbf{J}}}=\frac{\pi^4}{14\zeta(3)}, \tag{7}$$

which is material-independent, unlike the Ginzburg-Landau parameter $\kappa=\lambda/\xi$.

For the equations to refer to both superconducting and normal states the temperature dependence must be explicitly included. Calculations from the Usadel theory[24,25] gives the following boundary conditions at a material interface[26] (the first boundary condition corresponds to the continuity of pair conservation amplitude, while the second corresponds to supercurrent conservation):

$$\left[\overline{\psi}_{(2)}\right]_{Boundary}=\left[\overline{\psi}_{(1)}\right]_{Boundary}, \tag{8}$$

$$\left[\frac{\hat{\mathbf{n}}}{\rho_{(2)}}\cdot\left(\nabla-\frac{2ie}{\hbar}\mathbf{A}\right)\overline{\psi}_{(2)}\right]_{Boundary}=\left[\frac{\hat{\mathbf{n}}}{\rho_{(1)}}\cdot\left(\nabla-\frac{2ie}{\hbar}\mathbf{A}\right)\overline{\psi}_{(1)}\right]_{Boundary}, \tag{9}$$

where

$$|\overline{\psi}|^2=\left(\frac{T_c}{T}-1\right)|\psi|^2. \tag{10}$$

By substituting (10) into (1) and (2) we can obtain a form of the TDGL equations appropriate for both superconducting and normal states:

$$\frac{1}{\xi^2}\left(\frac{|\overline{\psi}|^2}{(T_c/T)-1}-1\right)\overline{\psi}+\left(\frac{\nabla}{i}-\frac{2e}{\hbar}\mathbf{A}\right)^2\overline{\psi}+\frac{1}{D}\left(\frac{\partial}{\partial t}+i\frac{2e}{\hbar}\varphi\right)\overline{\psi}=0, \tag{11}$$

$$\mathbf{J}_e=\frac{\hbar}{2e\mu_0\lambda^2(T_c/T)-1}\mathrm{Re}\left(\overline{\psi}^*\left(\frac{\nabla}{i}-\frac{2e}{\hbar}\mathbf{A}\right)\overline{\psi}\right)-\frac{1}{\rho}\left(\nabla\varphi+\frac{\partial\mathbf{A}}{\partial t}\right). \tag{12}$$

The first of these boundary conditions implies that $\overline{\psi}$ can be replaced by an alternative normalization $\hat{\psi}=C\overline{\psi}$ where C has the same value everywhere. Making the substitution

$$|\bar{\psi}|^2 = \left(\frac{T_{c(1)}}{T} - 1\right)|\hat{\psi}|^2, \tag{13}$$

restores Eqs. (1) and (2) for material 1 (in material 1 $\hat{\psi}=\psi$) while giving

$$\frac{1}{\xi_{(2)}^2}\left(\frac{T_{c(1)}-T}{T_{c(2)}-T}|\hat{\psi}|^2 - 1\right)\hat{\psi} + \left(\frac{\boldsymbol{\nabla}}{i} - \frac{2e}{\hbar}\mathbf{A}\right)^2\hat{\psi} + \frac{1}{D_{(2)}}\left(\frac{\partial}{\partial t} + i\frac{2e}{\hbar}\varphi\right)\hat{\psi} = 0, \tag{14}$$

$$\mathbf{J}_e = \frac{\hbar}{2e\mu_0\lambda_{(2)}^2}\frac{T_{c(1)}-T}{T_{c(2)}-T}\mathrm{Re}\left(\hat{\psi}^*\left(\frac{\boldsymbol{\nabla}}{i} - \frac{2e}{\hbar}\mathbf{A}\right)\hat{\psi}\right) - \frac{1}{\rho_{(2)}}\left(\boldsymbol{\nabla}\varphi + \frac{\partial \mathbf{A}}{\partial t}\right), \tag{15}$$

for material 2. Using the identities $(D_{(2)}/\xi_{(2)}^2)((T_{c(1)}-T)/(T_{c(2)}-T)) = D_{(1)}/\xi_{(1)}^2$ and $(\rho_{(2)}/\lambda_{(2)}^2)((T_{c(1)}-T)/(T_{c(2)}-T)) = \rho_{(1)}/\lambda_{(1)}^2$, Eqs. (14) and (15) can be rewritten in the $\varphi=0$ gauge as

$$\frac{\partial\hat{\psi}}{\partial t} = -\left[\frac{D_{(1)}}{\xi_{(1)}^2}\left(|\hat{\psi}|^2 - \frac{T_c - T}{T_{c(1)}-T}\right)\hat{\psi} + D\left(\frac{\boldsymbol{\nabla}}{i} - \frac{2e}{\hbar}\mathbf{A}\right)^2\hat{\psi}\right], \tag{16}$$

$$\frac{\partial \mathbf{A}}{\partial t} = \frac{\hbar\rho_{(1)}}{2e\mu_0\lambda_{(1)}^2}\mathrm{Re}\left(\hat{\psi}^*\left(\frac{\boldsymbol{\nabla}}{i} - \frac{2e}{\hbar}\mathbf{A}\right)\hat{\psi}\right) - \frac{\rho}{\mu_0}\boldsymbol{\nabla}\times\boldsymbol{\nabla}\times\mathbf{A}. \tag{17}$$

Here, D, T_c and ρ, without subscripts, represent the *local* values of diffusivity, critical temperature and resistivity. The equations can then be rewritten throughout the entire system (i.e., materials 1 and 2) in dimensionless units based on the properties of material 1, using

$$\boldsymbol{\nabla} = \frac{\boldsymbol{\nabla}'}{\xi_{(1)}}, \quad \frac{\partial}{\partial t} = \frac{\rho_{(1)}}{\mu_0\lambda_{(1)}^2}\frac{\partial}{\partial t'}, \quad \frac{2e}{\hbar}\mathbf{A} = \frac{\mathbf{A}'}{\xi_{(1)}}. \tag{18}$$

The unit of normalized length is the coherence length $\xi_{(1)}$, while normalized time is in units of the supercurrent time constant $\tau_{(1)}^{\mathbf{J}}$. The normalized magnetic field unit is the upper critical field:

$$H_{c2(1)} = \frac{\hbar}{2e\mu_0\xi_{(1)}^2}. \tag{19}$$

We can now apply the following normalization to get the dimensionless equations used in the rest in this paper:

$$\frac{\partial\hat{\psi}}{\partial t'} = \frac{1}{\zeta'}\left[\left(|\hat{\psi}|^2 - \frac{T_c - T}{T_{c(1)}-T}\right) + \frac{D}{D_{(1)}}\left(\frac{\boldsymbol{\nabla}'}{i} - \mathbf{A}'\right)^2\right]\hat{\psi}, \tag{20}$$

$$\frac{\partial \mathbf{A}'}{\partial t'} = \mathrm{Re}\left(\hat{\psi}^*\left(\frac{\boldsymbol{\nabla}'}{i} - \mathbf{A}'\right)\hat{\psi}\right) - \kappa_{(1)}^2\frac{\rho}{\rho_{(1)}}(\boldsymbol{\nabla}'\times\boldsymbol{\nabla}'\times\mathbf{A}'), \tag{21}$$

where the boundary conditions are Eqs. (8) and (9) with $\hat{\psi}$ substituted for $\bar{\psi}$.

B. Varying coating resistivity

The Ginzburg and Landau original paper[27] described a superconductor in terms of the two free parameters α and β, which can be expressed in terms of the coherence length ξ and penetration depth λ. Both ξ and λ are temperature dependent, and so together with the critical temperature T_c define the thermodynamic properties of any homogeneous isotropic superconductor as a function of field and temperature. The time-dependent Ginzburg-Landau equations add the diffusivity D and the normal-resistivity ρ to the equations, but D can be obtained from ξ and T_c via Eq. (3), while the ρ can be obtained from λ and T_c using Eq. (4), thus showing that introducing time dependence does not introduce any new free parameters. Hence ρ, D, and T_c also provide a complete set of variables.

In this paper we consider both simple normal metal coatings and bilayer coatings which include an additional weakly superconducting layer to represent a diffusion layer. Changing the resistivity of the normal metal coating leaves complete freedom in setting its diffusivity. In this paper the Fermi-level density of states $g(\varepsilon_F)$, given by

$$g(\varepsilon_F) = \frac{1}{2e^2D\rho}, \tag{22}$$

was held constant throughout the grid, while T_c and ρ were used to define material properties. This is appropriate if changes in resistivity are determined mainly by impurity concentration (and therefore by changes in D). In the bilayer (S'/N) coating simulations, T_c and ρ were varied linearly across the S' layer. Since the core superconductor in the computation is the critical part of the system, and in most relevant experiments is far larger than the coatings, the magnetization data were obtained from a sum over the core superconductor alone (i.e., not including the S' layer). The approach excludes the possibility that the data are disproportionally representative of the coatings.

III. COMPUTATIONAL METHOD

A. Symmetry problems

If a local energy minimum in a physical system can become a local maximum while equilibrium is maintained throughout, changes in the system cannot be described correctly without explicit consideration of symmetry breaking. Whereas an analytic calculation can check for the point at which a minimum becomes a maximum and then identify the correct minimum-energy equilibrium state, a time-dependent computation can get stuck at an energy maximum unless symmetry breaking is introduced. In a superconductor, both

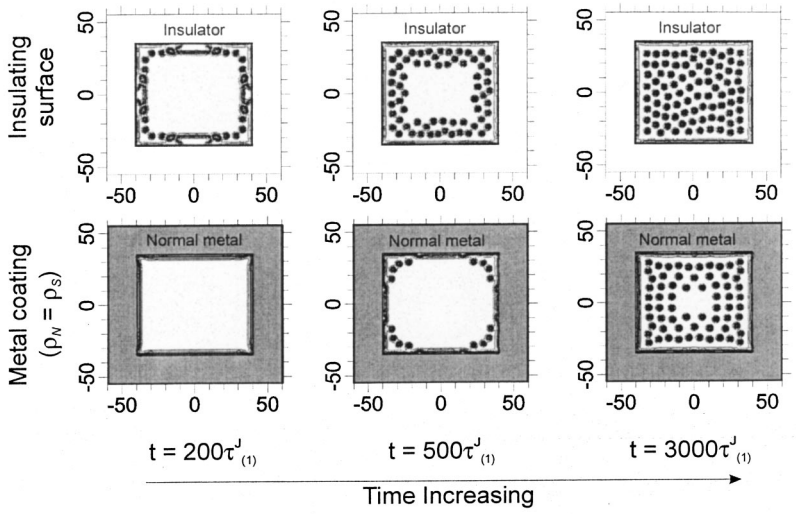

FIG. 1. Time evolution of $|\hat{\psi}|^2$ showing vortex entry into a $\kappa=2$ superconductor of dimensions $80\xi\times70\xi$ with an insulating surface and with a $\rho_N=\rho_S$, 20ξ thick metal coating (partly shown for clarity) and insulating outer surface. The applied magnetic field is increased above the initial vortex penetration field (i.e., to $H_p+0.01H_{c2}$) at $t=0$. Time frames at $200\tau^{\mathbf{J}}_{(1)}$, $500\tau^{\mathbf{J}}_{(1)}$ and $2000\tau^{\mathbf{J}}_{(1)}$ are shown. $|\hat{\psi}|^2$ contours are at intervals of 0.1.

the Meissner state and the normal state may be erroneously preserved if symmetry breaking is absent.

In the Meissner state of an infinitely long superconductor, every point along the edge is equivalent to every other point, which may mean that the superconductor remains trapped in this state even above H_p. We have addressed this symmetry problem by considering finite rectangular (where the corners break the symmetry) and circular (where roughness is imposed by the rectilinear discretization) superconductors. If the surface barrier is not weakened by the corners, H_p obtained from both rectangular and circular computations will agree with analytic values in the large-grid limit.

Similarly, if the superconductor becomes completely normal it is impossible for superconductivity to renucleate even if this is energetically favorable. When $\hat{\psi}$ is zero everywhere, $\partial\hat{\psi}/\partial t'=0$ [cf. Eq. (20)] and the normal state is erroneously preserved whatever the shape of the superconductor. Renucleation of superconductivity can be enabled by adding random Gaussian noise to both real and imaginary components of $\hat{\psi}$ after every 50 iterations. This noise is of mean zero and standard deviation 10^{-6}. Within the superconducting regime this noise has a negligible effect on the results, as noise 10^4 times more intense was found to have a negligible effect on the results[18] except for the time scale—more noise leads to faster equilibration.

B. Numerical method

Much of the existing TDGL computational work has been done using the simple explicit U-ψ method.[6,8,18] An explicit algorithm for solving partial differential equations involves calculating the time-derivatives based on existing data, and then advancing in time by a simple Euler step. Unfortunately, this method is very computationally expensive for diffusion equations such as the TDGL equations—as the explicit algorithm only considers nearest neighbors, the timestep δt between iterations must be shorter than the diffusion time across a cell of width δx for the algorithm to be stable.[28] Many of the calculations presented here would have required a $\delta t<0.001\tau^{\mathbf{J}}_{\mu(1)}$ had they been calculated using the U-ψ method, even for $\kappa=2$, and at high κ values even smaller δt values would have been needed, scaling as $1/\kappa^2$. In this paper we used a semi-implicit algorithm[3] which considers the effect of the entire grid on any given location, thus allowing a δt of up to $0.5\tau^{\mathbf{J}}_{\mu(1)}$, although for ρ_N/ρ_S values far from 1, δt values as low as $0.1\tau^{\mathbf{J}}_{\mu(1)}$ were needed for accuracy and stability. We note that to successfully use these much larger time steps, one of the link variables must be calculated first, and the new results used in calculating the second link variable. When the two link variables were calculated in parallel, even the semi-implicit algorithm became unstable. The order of link-variable calculation is switched on alternate iterations to preserve x/y symmetry as much as possible.

C. Optimizing the computation

In Schmid's dirty-limit TDGL theory, the ratio of the time constants $\zeta'=\pi^4/14\zeta(3)=5.78$, while in TDGL theory as obtained for superconductors dominated by paramagnetic impurities,[29] $\zeta'=12$. In Fig. 1, where the time evolution is of explicit interest, our calculation uses $\zeta'=5.78$. The remaining work in this paper considers equilibrium properties, where the time-dependent terms ultimately tend to zero. As a result, ζ' was set to 1 to reduce computational expense. We have confirmed that this setting of ζ' does not affect the results, while reducing computation times considerably—this is consistent with work in the literature.[8] In order to obtain the equilibrated magnetic properties, the applied magnetic field was ramped from one value to the next, and then held constant. The field increment was typically $0.05H_{c2}$, ramped over $100\tau^{\mathbf{J}}_{\mathrm{l}_{(1)}}$, although when obtaining precise H_p values much smaller increments were used. The equilibration time (typically $400\tau^{\mathbf{J}}_{\mu(1)}$, although this varied depending on the system) was determined by confirming the convergence of M to 3 significant figures.

In all computations included in this paper, a grid spacing of 0.5ξ in both x and y directions was used. H_p is dependent on grid size—it is higher for small superconductors, as the screening current on the near side of the superconductor which induces flux entry is partially cancelled by the oppo-

site screening current at the far side. This meant it was necessary to check that the grid size was large enough to obtain H_p results consistent with results in the literature for the insulating and extreme metallic limits. For the rectangular grid, for $\kappa=2$ the grid size was $50\xi\times40\xi$, with a 10ξ thick coating. For $\kappa=5$ calculations, a $100\xi\times80\xi$ grid with a 10ξ thick coating was used, $250\xi\times200\xi$ with a 20ξ coating for $\kappa=10$ and $625\xi\times500\xi$ for $\kappa=20$ with a 20ξ coating. For the circular superconductors referred to in Fig. 3, the diameters used were 50ξ for $\kappa=2$, 100ξ for $\kappa=5$, 250ξ for $\kappa=10$ and 500ξ for $\kappa=20$, with the same coating. The large grid sizes for $\kappa=10$ and $\kappa=20$ use up to 1 GB of RAM—to reduce the computational expense the superconductor was divided into symmetric quarters, and the computation was restricted to a single quarter. The same *S* grid sizes and *N* thicknesses are used in the bilayer coating calculations.

IV. RESULTS

A. Flux entry behavior

Figure 1 shows the time evolution of $|\hat{\psi}|^2$ as flux enters a superconductor with an insulating surface and a superconductor with a $\rho_N=\rho_S$ normal metal coating (the outer surface of the coating was set to be insulating). For each system, the superconductor was equilibrated in the Meissner state with an applied field of $H_p-0.01H_{c2}$ (where H_p is the minimum field at which flux entry occurs) then the field was increased to $H_p+0.01H_{c2}$. The mechanism of flux entry is quite different in the two cases—in the insulating surface case a continuous normal region forms at the edges which then breaks up into fluxons, while in the metal-coated superconductor individual fluxons enter the superconductor from the edge of the material where $|\hat{\psi}|^2$ has been depleted by the proximity effect. When the magnetization response was calculated for a superconductor with normal metal coatings of various thicknesses, it was found that any thickness above $2\xi_{(1)}$ gave the same result for H_p. This shows that the order parameter within the coating becomes negligible within $2\xi_{(1)}$ for $H\approx H_p$, and so the normal metal coatings used here can be considered to be infinitely thick. A metal coating slows the diffusion of fluxons into the superconductor compared to an insulating surface because H_p, and therefore the driving force on the fluxons, is lower for the metal-coated superconductor.

In the analytic work on initial vortex penetration, the nonsuperconducting side of the barrier is not explicitly considered. In both the insulating[17] and extreme metallic[14] limits, $\psi=0$ outside the superconductor, and the fluxons first nucleate just inside the superconductor. For a superconductor coated with a normal metal this leads to the question as to where current vortices first form. Figure 2 is a logarithmic contour plot for such a system. It consists of three main regions: an outer region in the normal coating dominated by noise where $|\hat{\psi}|^2<10^{-10}$, a second region containing screening currents which circulate near the superconductor-normal interface and exists in both regions and an inner region which contain a few fluxons, but where the order parameter is in most regions close to unity (Meissner state). It can be seen that there are small depressions of ψ within the normal metal layer, which have associated vortex currents. These proto-fluxons do not have quantized flux of ϕ_0 associated with them. We have found that unlike the two extreme limits considered analytically, the proto-fluxons first nucleate within the "noisy" region in the normal coating, then cross the screening current region into the superconductor.

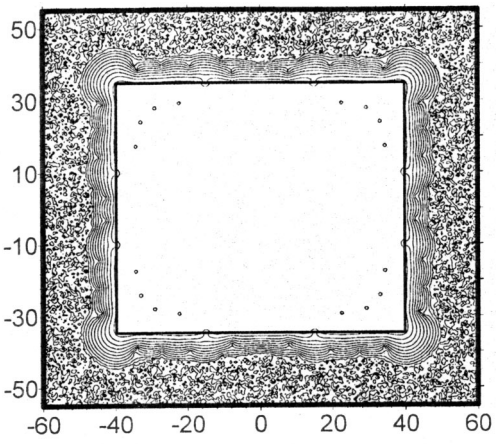

FIG. 2. Contour plot of $\log_{10}(|\psi|^2)$ for a $\kappa=2$ superconductor of dimensions $80\xi\times70\xi$ coated with a $\rho_N=\rho_S$, 20ξ thick normal metal and bounded by an insulating outer surface. The applied magnetic field was increased to above the initial vortex penetration field (i.e., to $H_p+0.01H_{c2}$) at $t=0$ and data obtained at $t=500\tau_{(1)}$. $\log_{10}(|\hat{\psi}|^2)$ contours are at intervals of 1—the outer region has random $\log_{10}(|\hat{\psi}|^2)$ due to noise.

B. Normal metal coatings

Figure 3 shows the complete magnetization characteristics for superconductors coated with insulator and with metals of various resistivities. The sample magnetization *M* was calculated by subtracting the applied magnetic field *H* from the internal magnetic field *B* (calculated by $\nabla\times\mathbf{A}$), and then averaging over the *S* region only (the demagnetization factor can be ignored for a 2D system). Adding a metal coating reduces the surface critical field H_{c3} from its insulating-surface value of $1.69H_{c2}$ to H_{c2} when $\rho_N\leqslant\rho_S$, consistent with the Hurault result.[13] (Note that superconductivity can persist in corners even above H_{c3}, as noted in the literature.[18]) The magnitude of the magnetic hysteresis decreases as ρ_N/ρ_S decreases, or as κ increases. However, the field dependence of the hysteresis is a property not only of the coating itself but also of the shape of the superconductor because in superconductors with small dimensions, fluxons which have already entered the superconductor impede the entry of further fluxons.[16] In contrast to the hysteresis, the initial vortex penetration field H_p is characteristic of the coating alone, and is considered in more detail below.

Figure 4 shows the results of H_p calculations for coating resistivity values ranging from $\rho_N=0.1\rho_S$ to $\rho_N=10\rho_S$ at κ values of 2, 5, 10, and 20. H_p was calculated for both rectangular (open symbols) and circular superconductors (closed symbols). It is clear that $H_p(\rho_N/\rho_S)$ has a minimum value ($H_{p(\min)}$) that is *lower* than the extreme metallic limit

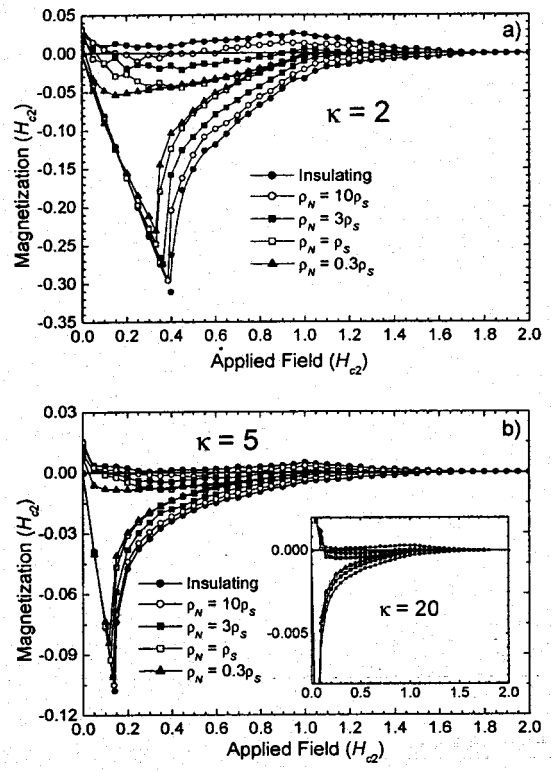

FIG. 3. Magnetization of a superconductor with an insulating surface and of superconductors with normal metal coatings of various resistivities (a) $\kappa=2$, (b) $\kappa=5$ with an inset for $\kappa=20$.

($H_p(0)$**)**, and that the resistivity ratio at which the minimum occurs $(\rho_N/\rho_S)_{opt}$, decreases as κ increases. The y axes in Fig. 4 have been scaled so that the extreme metallic ($\rho_N=0$) and insulating ($\rho_N=\infty$) limits are at the same positions for all values of κ (the H_p values at these two limits converge in the extreme high-κ limit[17]). The rectangular and circular H_p results agree to within a reasonable accuracy. We therefore conclude that the corners are not responsible for determining H_p in the rectangular superconductor and that the grid size is sufficiently large. The existing result that

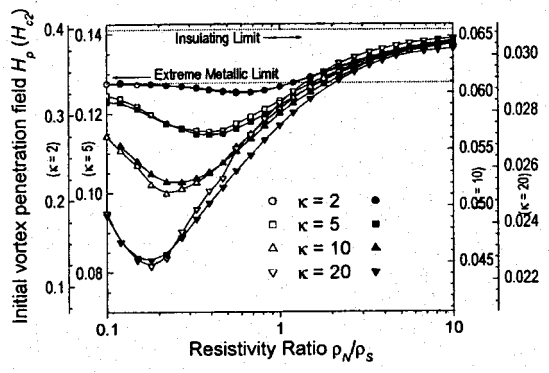

FIG. 4. Initial vortex penetration field H_p as a function of ρ_N/ρ_S for $\kappa=2$, 5, 10, and 20 for rectangular (open symbols) and circular (closed symbols) superconductors. The y-axes are scaled so that the asymptotic values of H_p in both the insulating and extreme metallic limits are at the same position for all κ values.

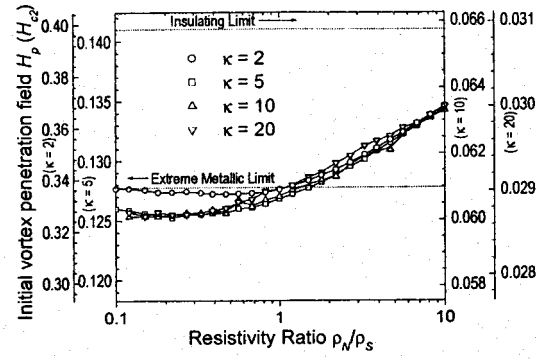

FIG. 5. Initial vortex penetration field H_p as a function of ρ_N/ρ_S for $\kappa=2$, 5, 10, and 20 for rectangular superconductors where $T_{c(N)}=-2T_{c(S)}$. The y-axes are scaled so that the asymptotic values of H_p in both the insulating and extreme metallic limits are at the same position for all κ values.

notches[8] reduce H_p and the observation in Fig. 1 that fluxons do not enter directly at corners suggest that convex features increase H_p, and in particular that corners do not weaken the surface barrier, and so that the computed H_p values in Fig. 4 are equivalent to values determined by the Bean-Livingston and Matricon calculations.

To confirm that the minimum in Fig. 4 is not specific to the conditions $T=T_{c(2)}=0$, Fig. 5 shows the effect of pair breaking on H_p. The same system is considered as in Fig. 4, but at $T=\frac{2}{3}T_{c(1)}$ and $T_{c(2)}=0$ (this is also equivalent to $T=0$ and $T_{c(2)}=-2T_{c(1)}$). In this system the minimum is attentuated considerably, as the pair-breaking forces $\hat{\psi}$ rapidly to zero in the normal metal, reinforcing the surface barrier for $\rho_N<\rho_S$, while weakening it for $\rho_N>\rho_S$. However, the minimum is not suppressed completely. The convergence of the data at high ρ_N/ρ_S in Figs. 4 and 5 suggests that in the $\rho_N \gg \rho_S$ limit, $[H_p(\rho_N/\rho_S)-H_p(0)]/[H_p(\infty)-H_p(0)]$ depends primarily on ρ_N/ρ_S and T, not κ.

Figure 6 focuses on the minima in the $H_p(\rho_N/\rho_S)$ characteristics in Fig. 4 (with some additional κ values), and demonstrates that $H_{p(\min)}$, and $(\rho_N/\rho_s)_{opt}$ have approximate power-law dependences. Figure 7 shows the ρ_N/ρ_S dependence of the hysteresis energy, which is calculated from the

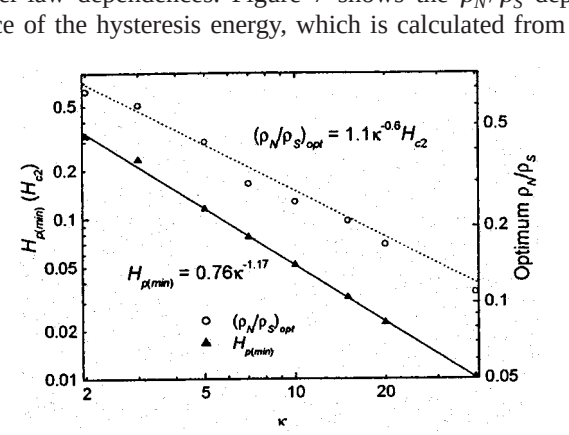

FIG. 6. Minimum initial vortex penetration field $H_{p(min)}$ (left axis) and required resistivity ratio ρ_N/ρ_S (right axis) as a function of κ.

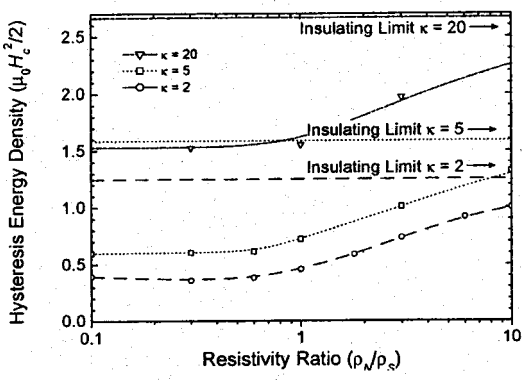

FIG. 7. Hysteretic energy density as a function of ρ_N/ρ_S at $\kappa=2$, 5, and 20.

area enclosed by the M-H loop. For $\rho_N > \rho_S$, the hysteresis energy increases with ρ_N/ρ_S, while for $\rho_N < \rho_S$ it is approximately independent of ρ_N/ρ_S. The minimum observed in the H_p characteristic does not appear in the hysteresis energy characteristic because hysteresis energy depends on both flux entry and flux exit, and the barrier for flux exit drops monotonically as ρ_N/ρ_S decreases in the important low field region. This cancels out the effect of the H_p minimum on the hysteresis energy.

C. Bilayer (S'/N) coatings

It is clear from the results presented so far that single normal metal coatings cannot destroy the surface barrier in any significant field range. The effect of a weakly superconducting S' layer between the S and N layers was therefore investigated with the intention of reducing the magnetic hysteresis further and obtaining reversible magnetic behavior over the widest possible field range.

Figure 8 shows examples of magnetization curves calculated for $\kappa=2$, bilayer coated superconductors. For an N layer with $\rho_N=\rho_S$, adding a 2ξ -thick S' layer has a minimal effect, while an S' layer at least 10ξ thick makes the magnetization essentially reversible above $0.4H_{c2}$. For an N layer with $\rho_N=10\rho_S$ adding an S' layer results in a less pronounced reduction of the hysteresis, and for a 2ξ-thick S' layer there is an anomalous increase in both H_p and hysteresis energy, which is discussed below. It may be noted that the calculations in Fig. 8(b) are more computationally expensive—not only does the large ρ_N require the simulation time step to be reduced, but the equilibration itself is slower—taking up to 10 times longer in normalized time than for a system with a simple normal metal coating.

In Fig. 8(a) the magnetization characteristics for S' thicknesses of 10ξ or more appear to be reversible for fields above $0.3H_{c2}$, which opens the possibility of the existence of an irreversibility field. Since the irreversibility field marks the point at which critical current density J_c becomes zero, it is an important issue both experimentally[30–32] and theoretically.[30,31] The magnetization irreversibility ΔM obtained from the data in Fig. 8(a) is plotted on a logarithmic scale in Fig. 9. It is clear that there is no evidence for a phase transition in high fields. For S' thicknesses of 20ξ, ΔM eventually becomes less than that resulting from a single fluxon for $H \geqslant 0.35H_{c2}$. A limited set of calculations for a much larger grid of $250\xi \times 200\xi$, where one fluxon would make a much smaller contribution to M, still showed a nonzero ΔM, thus confirming that the apparent irreversibility field in Fig. 8(a) is not the result of any phase transition.

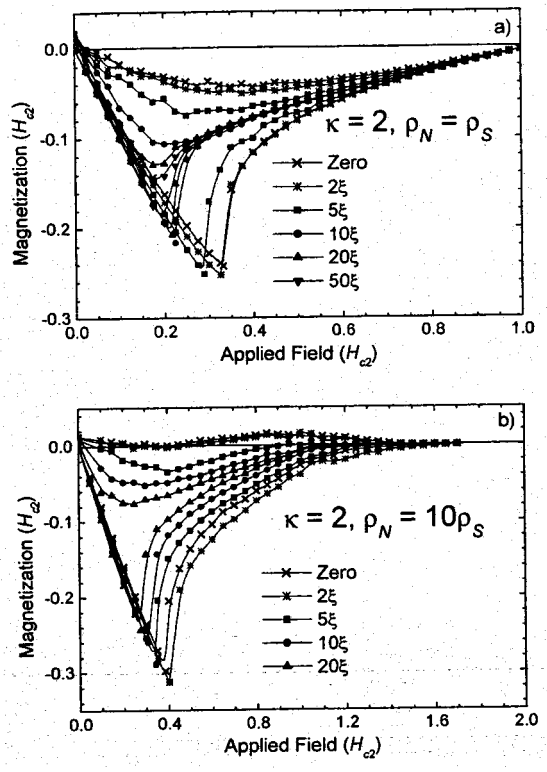

FIG. 8. Magnetization of a $\kappa=2$ superconductor coated with weakly superconducting S' layers of thicknesses up to 20ξ and an outer normal layer with (a) $\rho_N=\rho_S$ and (b) $\rho_N=10\rho_S$.

Figure 10(a) shows H_p as a function of the thickness of S' for $\kappa=2$ and ρ_N values of $0.1\rho_S$, ρ_S and $10\rho_S$. The anomalous increase in H_p first noted in Fig. 8(b) ($\rho_N=10\rho_S$) is found for

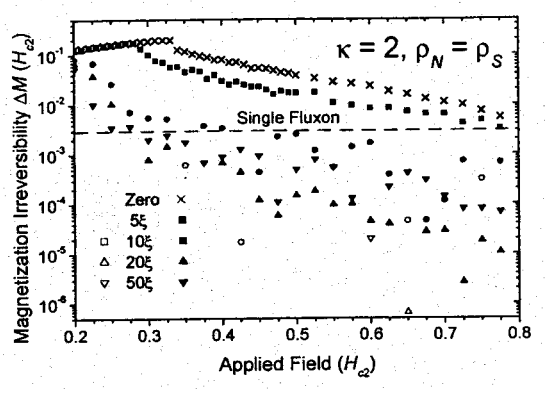

FIG. 9. Magnetization irreversibility on a logarithmic scale for $\kappa=2$ superconductors with $\rho_N=\rho_S$ normal metal coatings and S' layers of various thicknesses. (Negative values are indicated by open symbols.)

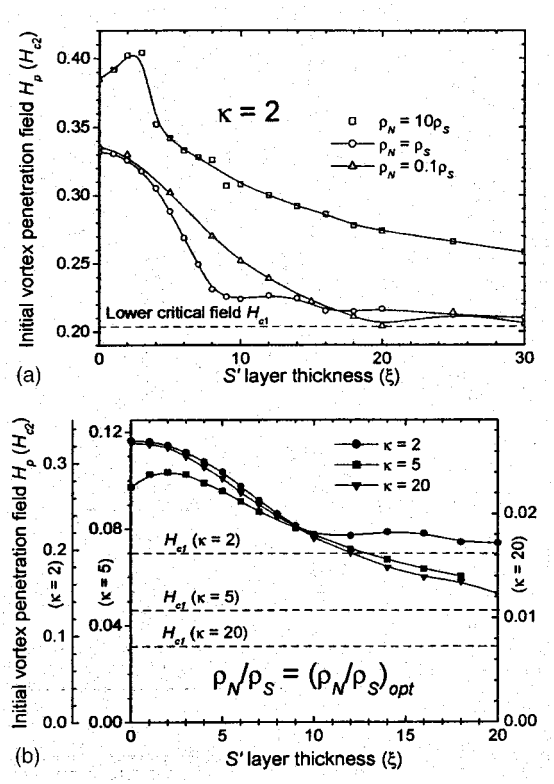

FIG. 10. Initial vortex penetration field H_p as function of S' thickness for (a) $\kappa=2$ superconductors with $\rho_N=\rho_S$ and $\rho_N=10\rho_S$ normal metal coatings, and (b) $\kappa=2$, 5, and 20 superconductors with coating resistivity given by $(\rho_N/\rho_S)_{opt}$. The y axes are normalized to H_p for a 10ξ-thick S′ layer.

S' thicknesses of 3ξ or less and confirmed to exist even for much finer grid spacings. In Eq. (20) for $\rho_N=10\rho_S$, diffusivity D is decreased within the S' layer, which lowers the kinetic energy term and thus increases $\hat{\psi}$ at the S'/S interface, increasing the energy penalty associated with moving fluxons into the superconductor. For S' thickness of 3ξ or less this effect dominates, resulting in the anomalous H_p increase, while for thicker S' layers, H_p decreases because the Bean-Livingston image force begins to dominate again. The initial vortex penetration field never reaches the lower critical field value[33] of $0.195H_{c2}$, but instead tends asymptotically to a somewhat higher value of $0.205\ H_{c2}$. This difference and hysteretic behaviour is found even for a 50ξ-thick S' layer [cf. Fig. 8(a)] and is discussed in the next section. Figure 10(b) demonstrates the effect of changing κ on the H_p characteristic as a function of S' thickness—for all values of κ there is a general trend of decreasing H_p as the S' thickness is increased, but again full reversibility is not achieved for thicknesses up to 20ξ.

V. DISCUSSION

A. The effects of coatings on H_p

The value of H_p is determined principally by two considerations. The first is the gradient of the order parameter at the interface of the superconductor. The dependence of H_p on the gradient explains the existence of the minimum. Both very low and very high ρ_N/ρ_S have high H_p as the interface boundary conditions force a steep gradient: on the N side of the interface for high ρ_N/ρ_S and on the S side for low ρ_N/ρ_S. This means that in both of these cases the Bean-Livingston "image force" is close to full strength. Close to $(\rho_N/\rho_N)_{opt}$, the screening supercurrent extends somewhat into the normal metal, weakening the image force and lowering H_p. This dependence of H_p on $\nabla\hat{\psi}$ also explains why adding a weakly superconducting S' layer reduces H_p, as ψ' is gradually reduced to zero over the width of the S' layer. The decrease in $(\rho_N/\rho_S)_{opt}$ as κ increases results from the second Ginzburg-Landau equation—at high κ values the screening current can penetrate farther into the normal metal, meaning gradients at the interface are optimized at a lower ρ_N/ρ_S value. The first Ginzburg-Landau equation only plays a minor role—it was found that changing the relation between D_N/D_S and ρ_N/ρ_S changed $H_{p(min)}$ but not $(\rho_N/\rho_S)_{opt}$.

The second consideration in determining H_p is the value of $\hat{\psi}$ itself at the interface. In the extreme metallic limit, $\hat{\psi}=0$ at the interface while in the insulating limit, $\hat{\psi}$ at zero field is the Meissner state value. $\hat{\psi}$ must be reduced to zero near the edge of the superconductor before any fluxons can enter, which results in a greater energy penalty for fluxon entry in the insulating limit, and thus a higher H_p than for the extreme metallic limit.[16] This "condensation energy" consideration also explains the anomalous increase in H_p observed in Fig. 8(b).

Finally we consider the general issue of the field dependence of the hysteretic magnetization data. Clearly, the reversible magnetization of a superconductor does not depend on its shape or size, provided that the separation between the parallel surface size is much larger than $\sim 20\lambda$ (λ= the penetration depth). The surface barrier contribution to the irreversible magnetization can be interpreted as a critical current along the surface of the superconductor per unit length in the z direction, and is thus also independent of shape and size. This means that the magnetization characteristics presented in Figs. 3 and 8 are completely general for a given κ value and surface, rather than being specific to a given shape or size. These calculations have also confirmed that thick smooth S' layers cannot completely destroy the surface barrier, to achieve complete reversibility surface defects such as notches or surface roughness are required.[8] It may also be noted that the magnitude of ΔM for the superconductors with insulating coatings can be approximated by

$$\Delta M \approx \frac{0.35}{\kappa^2\sqrt{H_{c2}}}(H_{c3}-H)^{3/2}. \tag{23}$$

If we consider a thin film conductor of thickness $\sim\lambda$, for example, of a high-temperature superconducting RABITS conductor,[32] the surface contribution to the average current density (J_c) is $\Delta M/\lambda$ which can be rewritten as $J_c \approx 0.64J_D/\kappa$ (where $J_D \approx H_c/\lambda$ is the theoretical upper limit known as the depairing current density[34]). Such high current densities are clearly of technological interest.

B. Comparison with experimental results

In many superconducting samples, the effect of the barrier is complicated by a combination of suppression of the superconductivity near the surface (due for example to oxidation), by roughness of the surface (the effect of notches on H_p has been investigated computationally[8]), or by the presence of twin boundaries or other defects. In such samples the effect of the surface barrier is most apparent in the immediate vicinity of H_{c1}, but obscured in higher fields by the effects of bulk pinning. Surface barriers strong enough for the characteristic asymmetric irreversibility shown in Fig. 3, with the almost-zero magnetization of the descending branch, has been observed in materials with surfaces which are flat on the scale of the coherence length, for example, in single crystals of YBCO (Ref. 35) and Bi-2212 (Ref. 36) as well as thin well-annealed samples of elemental niobium[36] and powdered MgB_2 (Ref. 37).

There has been relatively little experimental work on the effect of plating normal metals onto a superconductor with flat surfaces, although measurements reported on cylindrical samples of a niobium-zirconium alloy[38] showed a small decrease in magnetization irreversibility on plating with silver. The computational work presented in Sec. IV C of this paper shows that diffusing the boundary between a superconductor and its normal-metal coating radically reduces surface hysteresis (compare Fig. 3 with Fig. 8). This result has been observed experimentally in metallic interdiffusion experiments on a lead-thallium alloy[19] and in oxide-coated niobium.[20]

VI. CONCLUSIONS

This paper has considered the issue of coating superconductors with finite size single layer and bilayer coatings. The properties of superconductors of different κ and coated with materials with a range of resistivity and T_c have been calculated using the TDGL equations and discussed. Flux nucleation and penetration into a superconductor have been described, and the values for H_p, including conditions for it to be a minimum, have been reported. General characteristics for the hysteretic magnetization of large samples have been presented, which can be applied to coated materials of arbitrary shape.

ACKNOWLEDGMENTS

We express our gratitude to Lydia Heck, Duncan Rand, and Gerry Fuller for IT assistance. We also thank the CSAR National Supercomputing service for the use of their Origin machines.

[1] J. Crank and P. Nicolson, Proc. Cambridge Philos. Soc. **43**, 50 (1946).
[2] T. Frisch, Y. Pomeau, and S. Rica, Phys. Rev. Lett. **69**, 1644 (1992).
[3] T. Winiecki and C. S. Adams, J. Comput. Phys. **179**, 127 (2002).
[4] E. H. Brandt, Phys. Rev. B **58**, 6506 (1998).
[5] E. H. Brandt, Phys. Rev. B **60**, 11 939 (1999).
[6] M. Machida and H. Kaburaki, Phys. Rev. Lett. **71**, 3206 (1993).
[7] T. Winiecki and C. S. Adams, Phys. Rev. B **65**, 104517 (2001).
[8] D. Y. Vodolazov, Phys. Rev. B **62**, 8691 (2000).
[9] M. Machida and H. Kaburaki, Phys. Rev. Lett. **74**, 1434 (1995).
[10] M. Machida and H. Kaburaki, Phys. Rev. Lett. **75**, 3178 (1995).
[11] M. Machida and H. Kaburaki, Phys. Rev. B **50**, 1286 (1994).
[12] R. Kato, Y. Enomoto, and S. Maekawa, Physica C **227**, 387 (1994).
[13] J. P. Hurault, Phys. Lett. **20**, 587 (1966).
[14] C. P. Bean and J. D. Livingston, Phys. Rev. Lett. **12**, 14 (1964).
[15] P. G. De Gennes, Solid State Commun. **3**, 127 (1965).
[16] A. D. Hernández and D. Domínguez, Phys. Rev. B **65**, 144529 (2002).
[17] J. Matricon and D. Saint-James, Phys. Lett. **24A**, 241 (1967).
[18] R. Kato, Y. Enomoto, and S. Maekawa, Phys. Rev. B **47**, 8016 (1993).
[19] J. E. Evetts, Phys. Rev. B **2**, 95 (1970).
[20] G. P. van der Mey, P. H. Kes, and D. De Klerk, Physica B & C **95**, 369 (1978).
[21] A. Schmid, Phys. Kondens. Mater. **5**, 302 (1966).
[22] C.-R. Hu and R. S. Thompson, Phys. Rev. B **6**, 110 (1972).
[23] L. P. Gor'kov, Sov. Phys. JETP **10**, 998 (1960).
[24] K. D. Usadel, Phys. Rev. Lett. **25**, 507 (1970).
[25] K. R. Biagi, V. G. Kogan, and J. R. Clem, Phys. Rev. B **32**, 7165 (1985).
[26] Z. G. Ivanov, M. Yu. Kuprianov, K. K. Likharev, S. V. Meriakri, and O. V. Snigirev, Sov. J. Low Temp. Phys. **7**, 274 (1981).
[27] V. L. Ginzburg and L. D. Landau, Zh. Eksp. Teor. Fiz. **20**, 1064 (1950).
[28] W. H. Press, B. P. Flannery, S. A. Teukolsky, and W. T. Vetterling, *Numerical Recipes in* FORTRAN*: The Art of Scientific Computing*, 2nd ed. (Cambridge University Press, Cambridge, 1992).
[29] L. P. Gor'kov and G. M. Eliashberg, Sov. Phys. JETP **27**, 328 (1968).
[30] E. H. Brandt, Rep. Prog. Phys. **58**, 1465 (1995).
[31] G. Blatter, M. V. Feigelman, V. B. Geshkenbein, A. I. Larkin, and V. M. Vinokur, Rev. Mod. Phys. **66**, 1125 (1994).
[32] Y. Iijima and K. Matsumoto, Supercond. Sci. Technol. **13**, 68 (2000).
[33] E. H. Brandt, Phys. Rev. Lett. **78**, 2208 (1997).
[34] M. Tinkam, *Introduction to Superconductivity* (McGraw-Hill, Singapore, 1996).
[35] M. Konczykowski, L. I. Burlachkov, Y. Yeshurun and F. Holtzberg, Phys. Rev. B **43**, 13 707 (1991).
[36] P. K. Mishra, G. Ravikumar, V. C. Sahni, M. R. Koblischka, and A. K. Grover, Physica C **269**, 71 (1996).
[37] M. Pissas, E. Moraitakis, D. Stamopoulos, G. Papavassiliou, V. Psycharis, and S. Koutandos, J. Supercond. **14**, 615 (2001).
[38] H. A. Ullmaier and W. F. Gauster, J. Appl. Phys. **37**, 4519 (1966).